Phases in Interferometry

John D. Monnier

University of Michigan, Astronomy Department, Ann Arbor, MI 48109

Abstract

While interference fringes contain both amplitude and phase information, most interferometric results published to date focus solely on the amplitude data. This is because atmospheric turbulence corrupts the observed fringe phases, rendering them almost useless by themselves. Various techniques can be used to recover phase information and in this chapter we discuss the techniques of narrow-angle astrometry, differential phase, and phase closure for effectively recovering valuable and unique science from the otherwise-scrambled phase measurements. We focus especially on applications of closure phase made possible by current facilities.

Key words:

1 Phases in Optical Interferometry

1.1 Review

Earlier chapters have described the basic operation of interferometers and how interference fringes can be formed and their properties quantified. Figure 1 repeats the basic picture using a Young's two-slit experiment as a simple illustration of an interferometer. Here we see that the interference of starlight can be described by a fringe amplitude and phase and that the fringe phase depends on the angle of the incoming wavefronts entering the interferometer.

Thus, it is clear that measurement of fringe phase could be used for *astrometry*, precise determinations of stellar positions. Figure 2 shows a more realistic model of a ground-based interferometer, including a movable delay line that essentially acts to "point" the interferometer to different positions in the sky. By precisely measuring the delay line location required to find stellar fringes, one can calculate the incoming angle of the wavefronts and thus the stellar position on the sky.

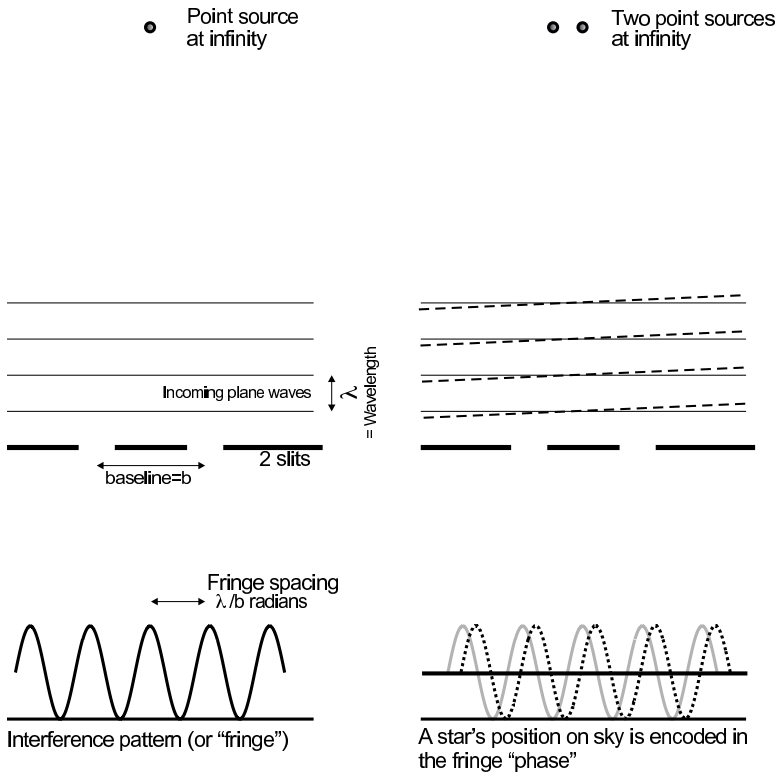

Fig. 1. The left panel shows a simple Young's two-slit interferometer response to a point source – the interference fringe can be characterized by an amplitude and phase. The right panels show how two different stars would produce fringes with different phase offsets, thus measurement of fringe phase is equivalent to a measurement of stellar position on the sky (in the absence of turbulence).

The Fourier phase of an interference fringe also encodes the spatial structure of a source, if the object is not a simple point source. The Van Cittert-Zernike theorem, described earlier in this book (see Chapter 1 in this volume by C. Haniff, and the classic textbook by Thompson et al., 2001), proves that the measure of fringe amplitude and phase can be directly related to the (complex) Fourier component of the object brightness distribution. For a point source, the phase encodes for location but for an arbitrary distribution the phase encodes for deviations from point-symmetry and these phases are needed for image reconstruction using aperture synthesis imaging techniques.

Unfortunately, simple application of interference fringe phases for astronomy is thwarted by atmospheric turbulence. Figure 3 shows how a dense pocket of air above one telescope introduces an exgtra time delay in the transmitted wavefront. This time delay induces a phase shift in the observed fringe pattern. In the visible and infrared, atmospheric turbulence causes many radians of phase delay on timescales of 5-20 milliseconds. This fringe blurring both ruins the phase information and also dramatically reduces interferometry sensitivity, since data must be taken in short exposures in order to effectively freeze the atmospheric turbulence.

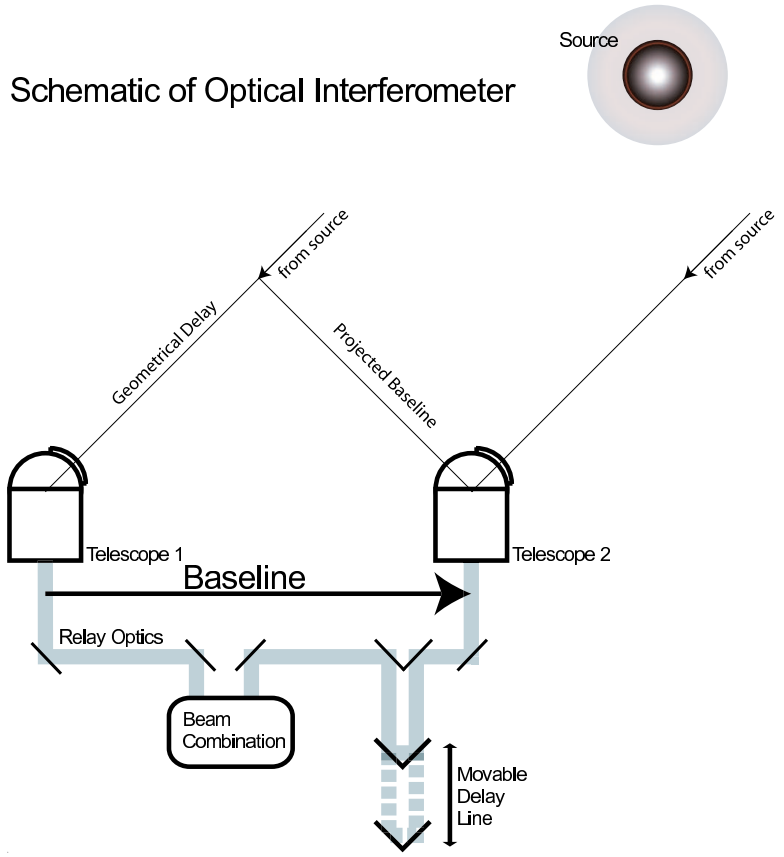

Fig. 2. Basic schematic of a realistic interferometer. By adjusting the movable delay line for maximum fringe coherence, the interferometer can be used to measure stellar positions (figure reprinted from Monnier, 2003).

In the next few sections we discuss techniques for overcoming the deleterious effects of the atmosphere.

1.2 Phase-Referencing and Narrow-Angle Astrometry

Phase errors caused by a time-variable atmosphere are not unique to visible and infrared interferometry – indeed, radio interferometers such as the Very Large Array (VLA) and the Very Large Baseline Array (VLBA) have long sought to overcome analogous propagation disturbances. The most widespread, practical, and effective technique is known as "phase referencing."

Atmospheric turbulence can be characterized both temporally and spatially. We already discussed the timescale of turbulence in the last section. Turbulence is also spatially correlated, such that wavefronts from objects located close together (in angle) on the sky experience similar phase delays. The scale of correlation depends on the layer height above the telescope array where the turbulence arises, and the angle of correlation is typically known as the

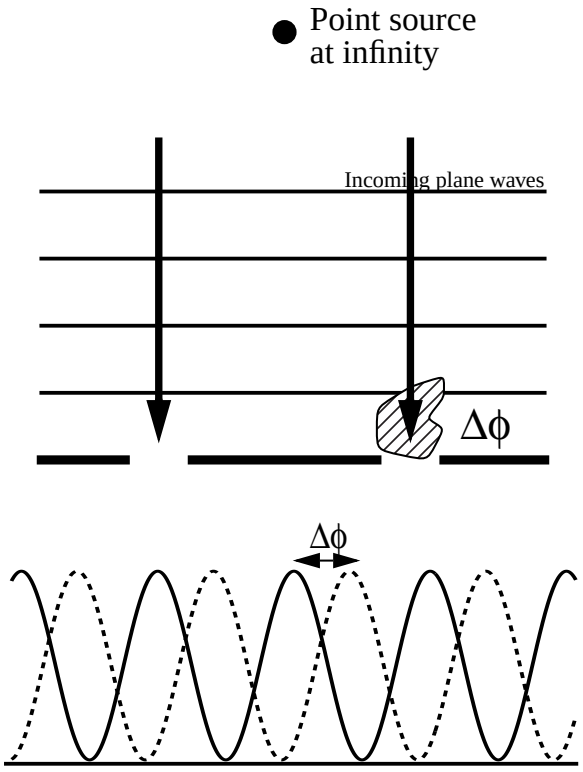

Fig. 3. Here we see that atmospheric turbulence introduces extra path length fluctuations, which induce fringe phase shifts. These phase shifts vary by many radians over short time scales (<<1 sec) effectively scrambling the Fourier phase information. In this chapter, we discuss methods for overcoming this loss of information (figure reprinted from Monnier, 2003)

isoplanatic patch (technically, the correlation length for an interferometer is different than for a single telescope – see Esposito et al., 2000, where the isopistonic patch is discussed). I recommend the Quirrenbach chapter in the 1999 Michelson Summer School proceedings (Quirrenbach, 2000) for a more technical description of of turbulence as it relates to interferometry.

In the radio, telescopes in the array can exploit these temporal and spatial correlations by quickly switching the pointing between a target and a "phase calibrator" located within a few degrees of the target. By monitoring the phase delays for the calibrator (which has a known location and brightness distribution), the induced phase errors can be calculated and then corrected for in the target datastream. Thus, one can measure the true target Fourier phase without undue corruption by the atmosphere.

Unfortunately, the coherence time in the visible/infrared is measured in milliseconds instead of minutes as in the radio, making it practically impossible to point and re-point the telescopes (let alone move the delay lines) between target and calibrator in this short time frame. Furthermore, the isoplanatic angle is much smaller than an arcminute compared to degrees in the radio,

meaning the probability of having a bright enough calibrator object near your target is generally small.

These obstacles can be partially overcome through the use of a "dual star module." In this technique, the dual-star module (sometimes known as a "field seperator") at each telescope picks off light from two nearby stars in the field-of-view *simultaneously* and directs the light into separate delay lines of the interferometer. One actively tracks the fringes on the brighter component and then feeds this correction to the second delay line. This acts as a kind of "adaptive optics" for interferometry, allowing (in theory) longer integrations on the secondary delay line and thus the possibility of observing much fainter objects. This technique has been applied at the Palomar Testbed Interferometer (Lane & Colavita, 2003). In addition, both the Very Large Telescope Interferometer (PRIMA) and Keck Interferometer are pursuing this approach to increase the interferometer sensitivity.

A special application of phase referencing above is "narrow-angle astrometry" (e.g., Shao & Colavita, 1992b,a). In this method, one measures the delay line difference between the two stars when using the dual-star module. This delay difference is a direct measurement of the angular distance on the sky along the baseline projection. Lane et al. (2000) demonstrated an rms error of 100 MICRO-arcsecond in a 7-night series of measurements on the binary 61 Cyg. More recently, this technique has been applied to close binaries (within a single diffraction-limited telescope beam) with remarkable astrometric precision (e.g., Muterspaugh et al., 2005).

1.3 Differential Phase

An increasingly-important phase retrieval technique in optical interferometry is "differential phase." In this method, the visibility amplitudes and phases are measured across many spectral channels simultaneously. In order to illustrate the method, consider observations of a strong emission line star (e.g., Hα for a Be star). The spectral line width ($\Delta\nu$) is very narrow compared to the emission frequency ν (e.g., $\nu/\Delta\nu > 1000$). Thus, the phase error introduced by the atmosphere is expected to be nearly constant across the spectral line (in the absence of dispersion, we expect $\mathrm{d}\Phi/\mathrm{d}\nu = 2\pi\tau$, where τ is the atmospheric time delay.) Thus, we can measure the visibility phase of the spectral line relative to the continuum by simply subtracting the continuum phase measured on either side of the spectral line.

To date, this procedure has been used in the visible for Hα (e.g., Mourard et al., 1989; Stee et al., 1995) and for NH_3 and SiH_4 in the mid-infrared (Monnier et al., 2000). Most recently the AMBER combiner on the VLTI has started

to produce results using differential phase in the near-IR – see the recent spectacular results of Weigelt et al. (2006). Some examples are considered in these proceedings.

While powerful, this method usually requires the presence of a strong spectral line, which limits the general applicability. A continuum version can also be carried out and this has been considered for the case of extrasolar planet detection (e.g., Akeson et al., 2000; Segransan, 2002), although there are systematic uncertainties in the dispersion correction due to the fluctuating water vapor content in the atmosphere. This technique will no doubt gain in importance thanks to the powerful spectroscopic capabilities of the VLT Interferometer with the AMBER combiner.

2 Introduction to Closure Phases

The rest of this paper will deal with another method for phase retrieval, phase closure, which can be applied more generally as long as the array can combine 3+ telescopes simultaneously. Here, we review the basic principles behind the closure phase and outline practical strategies for planning and subsequently interpreting observations using three-telescope arrays.

For simple sources such as binary stars, modelling of the closure phases can be used (theoretically) to reach unprecedented precision in model parameters, truly "Precision Interferometry." For more complicated objects (such as accretion disks around young stars), the ability to measure even a limited number of closure phases will lead to new astrophysical insight, before true interferometric "imaging" becomes standard practice. Taking full advantage of these new capabilities will require a deeper and more subtle understanding of the properties of closure phases, and this section hopes to communicate useful ways of thinking about closure phases in some common astrophysical contexts. Some material in this chapter can be found in proceedings of earlier interferometry summer schools (Monnier, 2000, 2002).

2.1 Derivation

In an interferometric array, amplitude and phase errors associated with telescope i can be conceptualized in terms of a complex gain, $\tilde{G}_i$, where the tilde is used to indicate a complex number endowed with both an amplitude and phase. In the radio, the electric field of the incoming radiation is directly measured at each telescope; in the visible/infrared, the field is not measured before interference, but rather is modified by the atmosphere and optics in each tele-

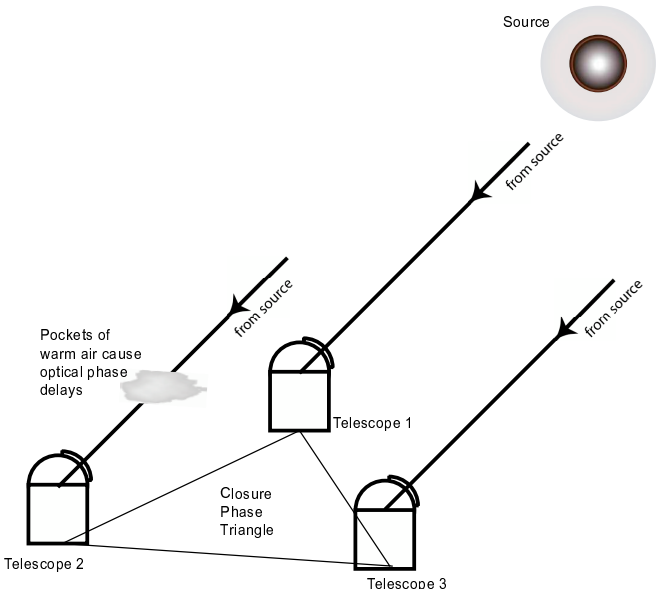

Fig. 4. Phase errors introduced at any telescope causes equal but opposite phase shifts in ajoining baselines, canceling out in the *closure phase* (see also Readhead et al., 1988; Monnier et al., 2006a).

scope before beam combination. In either case, the "measured" electric field can be represented as follows:

$$\tilde{E}_i^{\text{measured}} = \tilde{G}_i \tilde{E}_i^{\text{true}} = |G_i| e^{i\Phi_i^G} \tilde{E}_i^{\text{true}} \tag{1}$$

The amplitude of $\tilde{G}$ corresponds to the overall scale factor, collectively representing all telescope-specific effects which modify the intensity of the received stellar radiation, e.g. mirror reflectivity, detector sensitivity, local scintillation. The phase Φ_i^G encodes all telescope-specific phase shifts, such as those due changing optical pathlengths from thermal expansion/contraction or *atmospheric turbulence* above the telescope or along the beamtrain.

How do such errors effect the measurement of the complex visibility? When light from two telescopes i and j are interfered, the visibility $\tilde{\mathcal{V}}_{ij}$ is derived from the contrast of the resulting fringes. Using Eq. 1, we can see how the telescope-specific errors, represented by complex gains $\tilde{G}$, affect the measured visibility:

$$\text{Since} \qquad \tilde{\mathcal{V}}_{ij} \propto \tilde{E}_i \cdot \tilde{E}_j^*, \tag{2}$$

$$\tilde{\mathcal{V}}_{ij}^{\text{measured}} = \tilde{G}_i \tilde{G}_j^* \tilde{\mathcal{V}}_{ij}^{\text{true}} = |G_i||G_j| e^{i(\Phi_i^G - \Phi_j^G)} \tilde{\mathcal{V}}_{ij}^{\text{true}} \tag{3}$$

From Eq. 3, we can see mathematically that the measured phase of a detected fringe is shifted by the phase difference of the phase offsets at the individual

telescopes, as we previously discussed in §1 and showed in Figure 3. The phase shift is completely independent of the telescope separation, and only depends on telescope-specific phase delays (as in Eq. 3).

As previously emphasized, the loss of this phase information has serious consequences. Imaging of non-centrosymmetric objects rely on the Fourier phase information encoded in the interferometer fringes. Without this information, imaging can not be done except for simple objects such as disks or round stars.

2.2 Closure Phase and the Bispectrum

Consider Figure 4 in which a phase delay is introduced above telescope 2. This causes a phase shift in the fringe detected between telescopes 1-2, as just discussed in the last section. Note that a phase shift is also induced for fringes between telescopes 2-3; however, this phase shift is equal but *opposite* to the one for telescopes 1-2. Hence, the sum of three fringe phases, between 1-2, 2-3, and 3-1, is insensitive to the phase delay above telescope 2. This argument holds for arbitrary phase delays above any of the three telescopes. In general, the sum of three phases around a closed triangle of baselines, the *closure phase*, is a good interferometric observable; that is, it is independent of telescope-specific phase shifts induced by the atmosphere or optics.

The closure phase Φ_{ijk} can thus be written in terms of the three telescopes i,j,k in the triangle:

$$\Phi_{ijk} = \phi_{ij} + \phi_{jk} + \phi_{ki} \tag{4}$$

where ϕ_{ij} represents the measured Fourier phase for the baseline connecting telescopes i,j. Alternatively, the closure phase can be written in terms of the (u_0,v_0,u_1,v_1) in the Fourier (hyper-)plane where (u_0,v_0) represents the (u,v) coverage for baseline i, j in the triangle, where (u_1,v_1) represents the (u,v) coverage for baseline j, k in the triangle, and the last leg of the triangle can be calculated from the others since the sum of the 3 baselines must equal zero to be a "closure triangle." See definition and explanation put forward in documentation of the OI-FITS data format (Pauls et al., 2005).

The idea of closure phase was first introduced to compensate for poor phase stability in early radio VLBI work (Jennison, 1958). Application at higher frequencies was first mentioned by Rogstad (1968), but only much later carried out in the optical through aperture masking experiments (Baldwin et al., 1986; Haniff et al., 1987; Readhead et al., 1988). As of 2006, six different separate-element interferometers have succeeded in obtaining closure phase measurements, in the visible/infrared, first at COAST (Baldwin et al., 1996),

Table 1

Phase information contained in the closure phases alone

Number of Telescopes	Number of Fourier Phases	Number of Closing Triangles	Number of Independent Closure Phases	Percentage of Phase Information
3	3	1	1	33%
7	21	35	15	71%
21	210	1330	190	90%
27	351	2925	325	93%
50	1225	19600	1176	96%

soon after at NPOI (Benson et al., 1997) – most recently at IOTA (Monnier et al., 2004), ISI (Weiner et al., 2006), VLTI (Weigelt et al., 2006), and CHARA (Monnier et al., 2006b).

Another way to derive the invariance of the closure phase to telescope-specific phase shifts is through the *bispectrum*. The bispectrum $\tilde{B}_{ijk} = \tilde{\mathcal{V}}_{ij}\tilde{\mathcal{V}}_{jk}\tilde{\mathcal{V}}_{ki}$ is formed through triple products of the complex visibilities around a closed triangle, where ijk specifies the three telescopes. Using Eq. 3, we can see how the telescope-specific errors affect the measured bispectrum:

$$\tilde{B}_{ijk} = \tilde{\mathcal{V}}_{ij}^{\text{measured}}\,\tilde{\mathcal{V}}_{jk}^{\text{measured}}\,\tilde{\mathcal{V}}_{ki}^{\text{measured}} \tag{5}$$

$$= |G_i||G_j|e^{i(\Phi_i^G-\Phi_j^G)}\tilde{\mathcal{V}}_{ij}^{\text{true}} \cdot |G_j||G_k|e^{i(\Phi_j^G-\Phi_k^G)}\tilde{\mathcal{V}}_{jk}^{\text{true}} \cdot |G_k||G_i|e^{i(\Phi_k^G-\Phi_i^G)}\tilde{\mathcal{V}}_{ki}^{\text{true}} \tag{6}$$

$$= |G_i|^2|G_j|^2|G_k|^2\tilde{\mathcal{V}}_{ij}^{\text{true}} \cdot \tilde{\mathcal{V}}_{jk}^{\text{true}} \cdot \tilde{\mathcal{V}}_{ki}^{\text{true}} \tag{7}$$

From the above derivation, one can see that the bispectrum is a complex quantity whose phase is identical to the closure phase. The use of the bispectrum for reconstructing diffraction-limited images was developed independently (Weigelt, 1977) of the closure phase techniques, and the connection between the approaches elucidated only later (Roddier, 1986; Cornwell, 1987).

For N telescopes, there are "N choose 3," $\binom{N}{3} = \frac{(N)(N-1)(N-2)}{(3)(2)}$, possible closing triangles. However, there are only $\binom{N}{2} = \frac{(N)(N-1)}{2}$ independent Fourier phases; clearly not all the closure phases can be independent. The number of *independent* closure phases is only $\binom{N-1}{2} = \frac{(N-1)(N-2)}{2}$, equivalent to holding one telescope fixed and forming all possible triangles with that telescope. The number of independent closure phases is always less than the number of phases one would like to determine, but the *percentage* of phase information retained by the closure phases improves as the number of telescopes in the array increases. Table 1 lists the number of Fourier phases, closing triangles, independent closure phases, and recovered percentage of phase information for telescope arrays of 3 to 50 elements. For example, approximately 90% of the phase information is recovered with a 21 telescope interferometric array (e.g., Readhead et al., 1988). This phase information can be coupled with other

image constraints (e.g., finite size and positivity) to reconstruct the source brightness distribution.

2.3 General Properties of Closure Phases

Before we explore the closure phase for specific examples, I will summarize the most general properties here:

(1) The closure phases are independent of all *telescope-specific* phase errors. The measurement of non-zero closure phases from a point source result from having non-closing triangles or phase delays after splitting beams.
(2) Closure phases are not sensitive to an overall translation of the image.
(3) The bispectrum is real for sources with point-symmetry. That is, the closure phases are always 0 or 180 degrees. Detection of other angles implies the object's intensity distribution is *skewed*.
(4) Object must be resolved ($\Theta \gtrsim \frac{1}{2}\lambda/B$) in order to have a non-zero closure phase. For marginally resolved objects Closure Phase $\propto$ (Baseline)^3, while Phase $\propto$ (Baseline). See discussion in Lachaume (2003) and Monnier et al. (2006a).

2.4 Simple Example: a Binary

Let us start by analyzing a simple case and one which is scientifically relevant. How do the closure phases behave for a binary?

Since the closure phases are independent of the phase center (from Closure Phase Property #2), one can strategically place the origin in order to more easily determine the Fourier phases for a given brightness distribution. For example, consider the equal binary system depicted in Figure 5. The complex visibility can be easily written by choosing the origin midway between the two components. Note the abrupt phase jump when the visibility amplitude goes through a null. These discontinuities are smoothed out when the two components are not precisely equal.

But what about the closure phases? Since a closure phase is simply a sum of three phases, we can immediately see that all the closure phases must be either 0° or 180° (Closure Phase Property #3). In fact, this is true not just for equal binaries, but *any point-symmetric brightness distribution*. This is easily proven: by placing the origin (phase center) at the location of point-symmetry, then we can make the imaginary part of the Fourier transform disappear (i.e., all odd basis functions must vanish). Hence, the phases of *all* (non-zero) Fourier components must be either 0° or 180° .

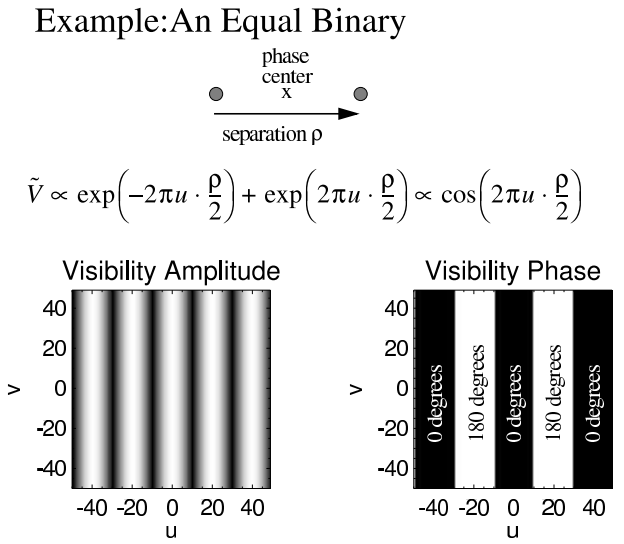

Fig. 5. This figure shows the complex visibility for an equal binary system. With the above choice for the phase center, the Fourier phases can be represented simply. Notice the abrupt phase jumps when visibility amplitude goes through a null.

For an equal binary then, we would expect to see abrupt closure phase jumps between 0° and 180° if one of the baselines traverses a null in the visibility pattern. This indeed has been observed with the NPOI interferometer (Benson et al., 1997). It is easy to show that the binary separation (and brightness ratio) can be determined from the closure phase information alone.

How would this look to an interferometer? Figure 6 shows an example interferometer layout (here modelled for IOTA). Figures 7 & 8 show the visibilities and closure phases that would be measured for binaries with different brightness ratios. It is not surprising that the "nearly equal" binary case shown on the right panels of Figure 7 resemble the pattern for the equal binary case,

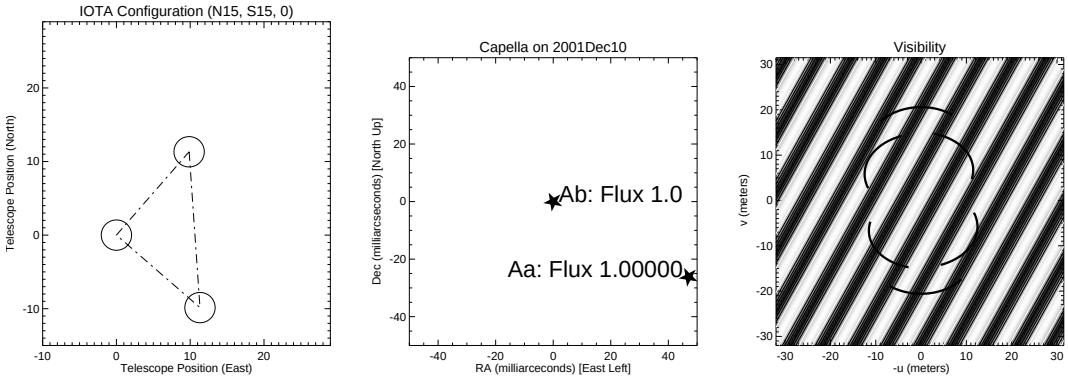

Fig. 6. The left panel shows the telescope positions used for calculating the visibility and closure phase signal of the binary geometry shown in the center panel. The right panel shows the binary visibility pattern projected onto the (u,v)-plane, with the observing (u,v)-tracks marked (6 hours of observing around transit). These observing tracks are adopted for the next two figures.

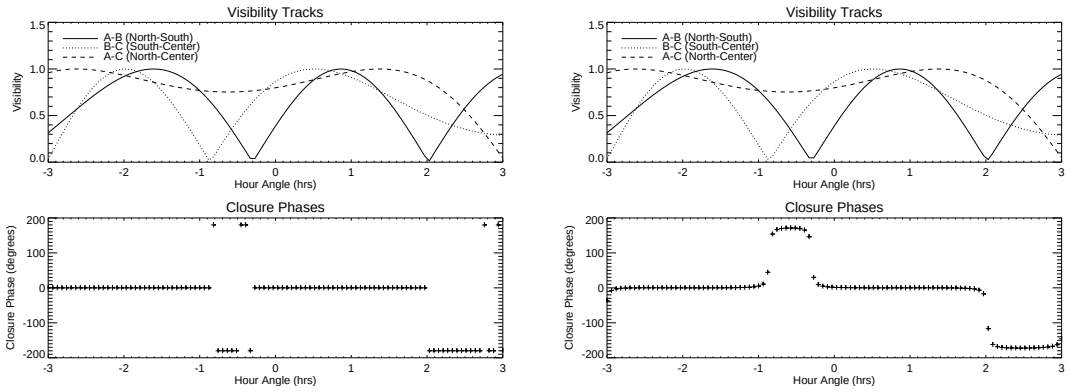

Fig. 7. The left panels shows the visibility data (top) and closure phases (bottom) of an equal binary during the the observations described in Figure 6. The right panels show the same for a slightly unequal binary (1 to 1.05). Note how the closure phases smoothly change from 0° to nearly 180° , as you would expect for a "nearly" point-symmetric object.

except the abrupt 180° transitions are now smoothed over, and the closure phase does not quite reach 180° anymore.

Figure 8 explores the consequences for the unequal binary case. We see that the magnitude of the closure phase (in radians) is roughly equal to the "amount" of asymmetry, which for a binary star is equal to the brightness ratio. Interestingly, this is also the same magnitude for the measurements of photocenter shifts in astrometric searches of planets, and thus high precision closure phase measurements could be a a potentially powerful tool for discovering faint companions to bright stars (such as the hot jupiters discovered in radial velocity surveys).

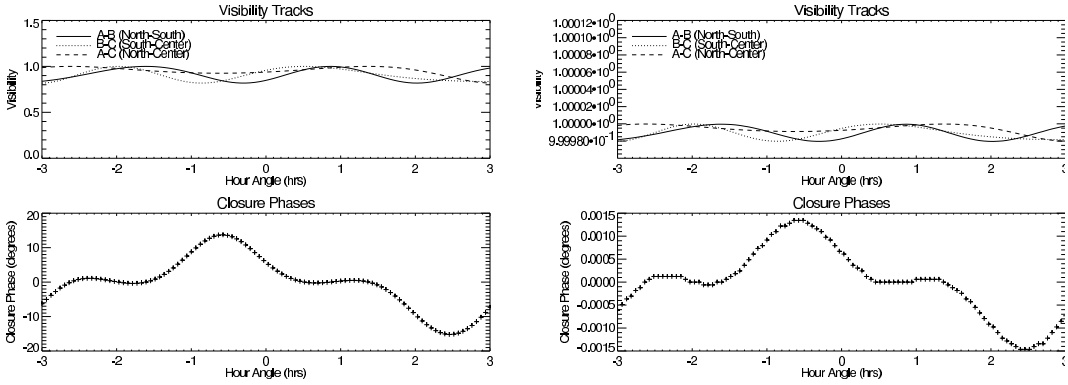

Fig. 8. Same as last figure, but for very unequal binaries. The left panels shows the visibility data (top) and closure phases (bottom) for a binary with flux ratio of 10. The right panel shows the same binary, but for a flux ratio of 100000 (which might be reasonable for a planet). Note that the magnitude of the closure phase signal is of the same order of magnitude (in radians) as the flux ratio, 1×10^{-5}.

2.5 Related "Closure" Quantities

2.5.1 Differential Closure Phase

The use of "Differential Phase" has already been discussed in §1.3 where the concept was to calibrate for the atmospheric phase delays in the interferometer by measuring the fringe phases as a function of wavelength. This technique is potentially very powerful, but is subject to uncertainties in the atmospheric dispersion when used over a wide bandpass.

Calibration of the closure phase might also benefit from using multi-wavelength measurements, since a "differential" closure phase might be stable to a variety of systematic errors (such as long term drifts in the optics). Since the closure phase is more immune to the uncertainties in dispersion, it could be used for many of the same applications planned for "differential phase," such as detecting exoplanets (Beuzit et al., 2006).

2.5.2 Closure Differential Phase

Unfortunately, one limitation of differential phase (and differential closure phase) is that it requires some assumptions about the source structure you are observing. For instance, if one measures the fringe phase in a spectral line compared to the surrounding continuum, one must know *a priori* the intrinsic fringe phase of the continuum in order to interpret the "differential phase." If the continuum source is expected to be unresolved, then one can safely assume the continuum fringe phase is zero and there is no problem.

However, consider observing an infrared emission line formed in a jet around a young stellar object. One would expect the near-infrared continuum to have significant contributions from dust scattering and thermal emission. Thus, one can not assume the continuum is unresolved. Further, one might expect the emission to be fairly complicated in morphology, thus the differential phase measured in the spectral line will be difficult to interpret. One would have to first make a continuum image, a difficult task with current arrays.

However, Figure 9 introduces the Closure Differential Phase. For each of the three baselines, one can measure the complex visibility in the emission line and in the neighboring continuum. By subtracting these complex quantities, one can isolate the complex visibility of the emission component, albeit corrupted by the atmospheric delay. However, one can form the closure phase using this differential phase measurement, and thus measure the closure phase of the emission component independent of the continuum. The forming of the closure phase using a kind of differential phase motivates the name "closure *differential phase*." Note that this differential phase is not the traditional differential

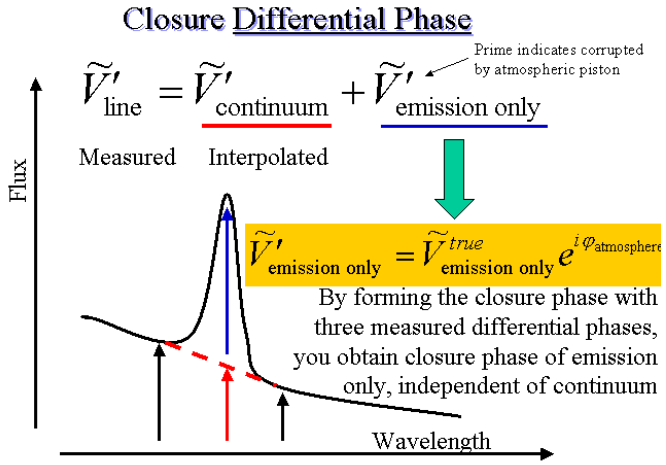

Fig. 9. Explanation of the "Closure Differential Phase."

phase, but rather results from the differencing of the complex visibilities in and out of the line, *not* merely differencing the fringe phases. Since the spectral line emission might be simpler than the continuum, for example in a jet, this method could be potentially useful when it is not feasible to make an image of the continuum.

2.5.3 Closure Amplitudes

When one has four or more telescopes, another important closure quantity can be formed: the *closure amplitude*. The closure amplitude is constructed to be independent of the telescope-specific gain amplitudes. The closure amplitude A_{ijkl} can be defined a variety of ways, but here it is defined in terms of four telescopes $ijkl$:

$$A_{ijkl} = \frac{|\tilde{\mathcal{V}}_{ij}^{\text{measured}}||\tilde{\mathcal{V}}_{kl}^{\text{measured}}|}{|\tilde{\mathcal{V}}_{ik}^{\text{measured}}||\tilde{\mathcal{V}}_{jl}^{\text{measured}}|} \tag{8}$$

$$= \frac{|\tilde{G}_i||\tilde{G}_j||\tilde{\mathcal{V}}_{ij}^{\text{true}}||\tilde{G}_k||\tilde{G}_l||\tilde{\mathcal{V}}_{kl}^{\text{true}}|}{|\tilde{G}_i||\tilde{G}_k||\tilde{\mathcal{V}}_{ik}^{\text{true}}||\tilde{G}_j||\tilde{G}_l||\tilde{\mathcal{V}}_{jl}^{\text{true}}|} \tag{9}$$

$$= \frac{|\tilde{\mathcal{V}}_{ij}^{\text{true}}||\tilde{\mathcal{V}}_{kl}^{\text{true}}|}{|\tilde{\mathcal{V}}_{ik}^{\text{true}}||\tilde{\mathcal{V}}_{jl}^{\text{true}}|} \tag{10}$$

In the radio, this is an important quantity and can be used to compensate for detector gain fluctuations and changing antenna efficiencies. However in the visible and infrared regimes, varying fringe amplitudes are often not caused by telescope-specific gain changes (such as scintillation), but rather arise from baseline-dependent decorrelation effects related to atmospheric turbulence. Hence, the closure amplitude has not been very important to consider for

optical interferometers. Recent advances, such as the use of spatial filtering, high-order adaptive optics systems and fast fringe-tracking, may make this quantity quite interesting in the future.

3 Science with Closure Phases

3.1 Precision Interferometry with Closure Phases

The precision of measured visibility amplitudes is usually limited by calibration of changing atmospheric conditions. Because the the closure phase is largely independent of atmospheric seeing, it is possible that closure phases will be measured with a greater precision than has been possible for visibility amplitudes. Thus model parameters for simple sources could be vastly improved by using well-calibrated closure phases.

Of course, not all simple sources have significant closure phase signals. For instance, the closure phases from a limb-darkened disk only vary across visibility nulls, thus closure phases are useless for precision measurements of limb-darkening. However, there are a number of simple sources which do lend themselves to modeling of the closure phases:

- Non-equal binary stars can be measured using precise closure phases. The separation, brightness ratio and even component diameters can be extracted by the closure phases. High signal-to-noise techniques could increase the magnitude ratio detectable using interferometry, perhaps enough to detect some planets, the hot jupiters. However, beware of systematic errors, such as from bandwidth-smearing effects (Zhao et al., 2007).
- While pulsating single stars do not have a time-changing closure phase signal (except beyond the first null), a pulsating star in a binary system will. For instance, a Cepheid changing size and brightness in a binary system could be measured using the time-changing closure phases.
- With good interferometer sensitivity, one could observe crowded fields. The closure phases could help immensely in performing narrow angle astrometry of the various components (i.e., parametric imaging), and could be used to study dynamics and proper motions.

3.2 Qualitative Astrophysics with Closure Phases

In the infrared, many targets will have significant contributions from dust shells which may be clumpy, complicated, and not representable by a simple

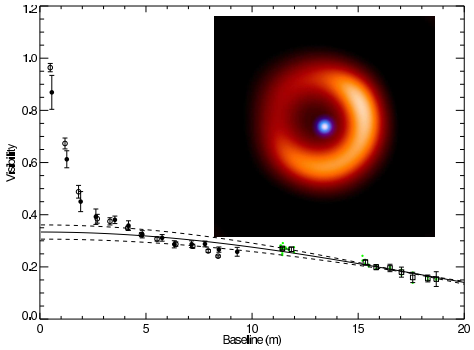

Fig. 10. A common case encountered in infrared interferometry is a star surrounded by a dust shell. This figure shows an example image and corresponding visibility curve. The important point is that the short baselines are probing the large scale structure of the object (the dust shell), while the long baselines resolve out the dust and only "see" the underlying star.

model. Without good aperture synthesis imaging capability, why should we observe such sources with, for example, just a 3-telescope interferometer?

Closure phases can discover qualitatively new information about some objects, much like measuring the polarization. Also as for polarization, the result is "informative, but not unambiguous." In this section, I will discuss how to use closure phase measurements with a 3-telescope array to discover fundamentally new things about your target. In this case, I will use the prototypical case of a "dust shell + star" as illustrated in Figure 10

There are four different kinds of closure triangles you might imagine employing to probe different aspects of this source. These are listed and described in Figure 11.

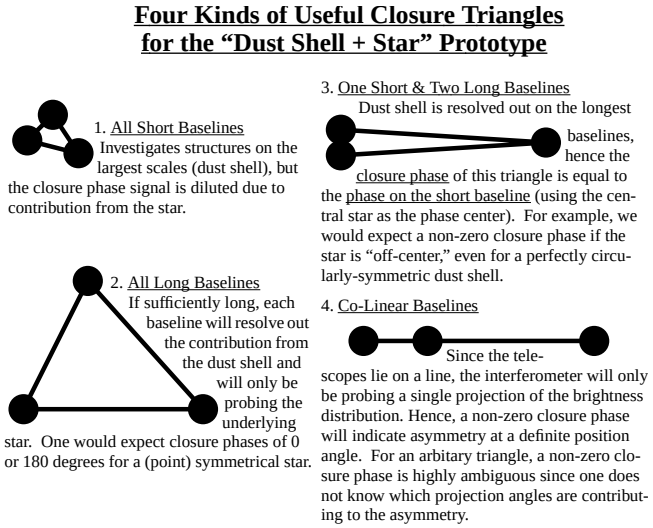

Fig. 11. This figure illustrates four important kinds of closure triangles.

3.2.1 Implications

Depending on your science goals, you would employ different triangles for your observations. Here are some examples:

(1) Goal: Find "interesting" young stellar objects for the subject of an intensive series of observations meant to image the accretion disk. Since YSO disks are pretty small (<5 mas), one could survey a large number of targets with relatively long baselines. To optimize one's sensitivity to "asymmetric" structure, I would recommend a large equilateral triangle to look for any kind of asymmetry. Our group at IOTA recently published the first such YSO closure phase survey (Monnier et al., 2006a).

(2) Goal: We already know an interesting target, and we want to see if the asymmetry is related to something else about the system. If you have some idea what the asymmetries might be (say from direction of previously seen jet, bi-polar outflow, or a known companion), then set up some linear arrays to probe the different position angles to (dis)prove that the asymmetries are related to these directions. Note that earth rotation will rotate your linear array through a range of position angles and so will not necessarily require many configuration changes (telescope relocations). Consider the interesting case of AB Aur, where IOTA found evidence for a disk hotspot (Millan-Gabet et al., 2006) using a short-baseline triangle!

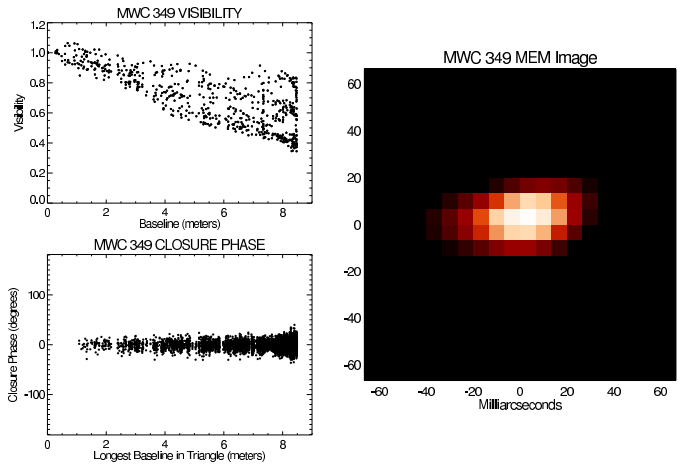

Fig. 12. This figure shows actually measured visibilities and closure phases for the young stellar object MWC 349. One can see directly from the visibilities that the source is highly elongated. However, the small (near zero) closure phases show the source is point-symmetric. Even without imaging (right panel), we could have guessed this source would look like a symmetric (edge-on) disk.

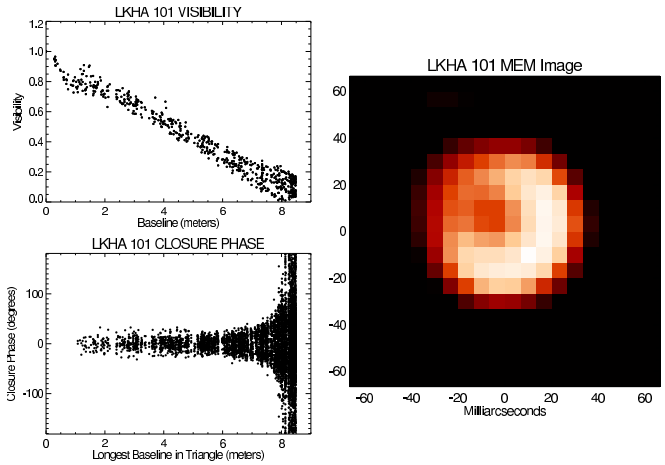

Fig. 13. This figure shows actually measured visibilities and closure phases for the young stellar object LkHα 101. One can see directly from the visibilities that the source is not highly elongated in any single direction. However, the large closure phases measured in triangles with long (>7 m) baselines show that there is highly asymmetric structure on small scales. The right hand panel shows the reconstructed image, which is indeed consistent with these qualitative features: an emission ring which is brighter on one side (i.e., skewed).

3.3 Examples

In Figures 12 & 13, we show examples of visibilities and closure phases based on actual results from aperture masking (Tuthill et al., 2001; Danchi et al., 2001). The large number of data points were made possible by masking the Keck Telescope (Tuthill et al., 2000), and allowed images to be reconstructed. Note the bottom left panel shows all the closure phases plotted against the longest baseline length in the corresponding closure triangle. In such a plot, one expects near-zero closure phases until there is enough resolution (long enough baselines) to resolve any asymmetric structure present (Closure Phase Property #4). We analyze the data for each source in the corresponding figure captions.

3.4 YSO disks with realistic interferometer

While the aperture masking examples are interesting, let us consider how the observations are different for a realistic 3-telescope interferometer. Figure 14 shows how IOTA might see a young stellar object. Indeed, the closure phase can be seen to vary with the angular resolution of the interferometer and the baseline orientations. I refer the interested reader to Monnier et al. (2006a) for detailed discussion of considerations for observing YSOs in search of closure phase signals.

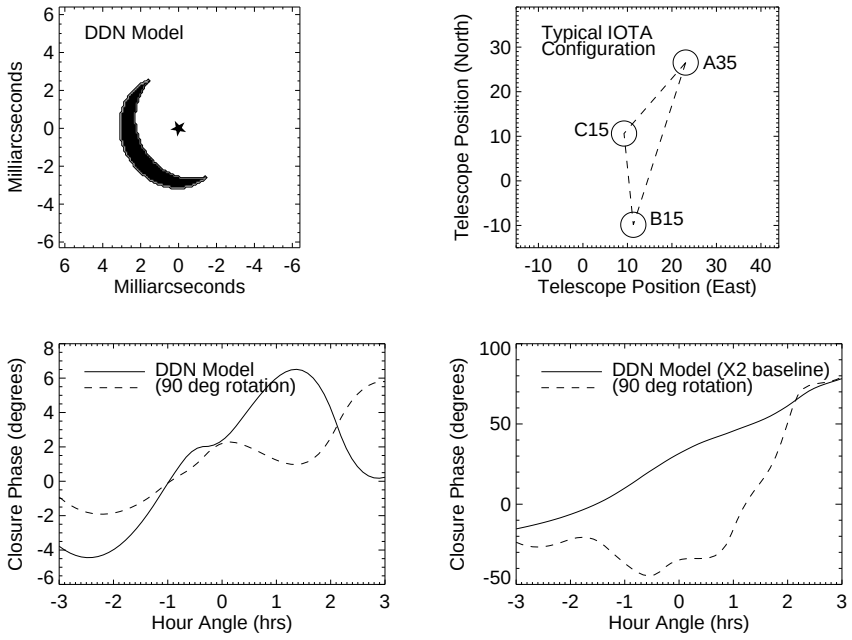

Fig. 14. This figure shows how the closure phase measured for disk emission strongly depends on the angular resolution and the orientation angle of the baselines w.r.t. the disk asymmetry. Please see Monnier et al. (2006a) for a complete discussion of this figure.

4 Imaging with Closure Phases

There is no space in this short chapter to discuss strategies for imaging with closure phases. This topic was touched on by Chris Haniff in an earlier chapter, and we refer the interested reader to his excellent introduction or to the classic text by Thompson et al. (2001). In addition, I refer you to the CHARA technical report by Tuthill & Monnier (2000), which attempted to answer the question "What is the minimum number of telescopes needed to do aperture synthesis imaging with closure phases?"

5 Conclusions

Long-baseline interferometers have only just started to exploit the science potential of fringe phases. This chapter outlined some of the most promising approaches that are coming into standard use at the current-generation of

interferometers, such as NPOI, VLTI, Keck, and CHARA. Soon, true imaging interferometry should be possible as the number of simultaneously-used telescopes increase at current facilities.

Acknowledgements
I recognize interesting and thought-provoking discussions with Chris Haniff, Dave Buscher, and John Young on various aspects of closure phase measurement and imaging theory.

References

Akeson, R. L., Swain, M. R., & Colavita, M. M. 2000, in Proc. SPIE Vol. 4006, p. 321-327, Interferometry in Optical Astronomy, Pierre J. Lena; Andreas Quirrenbach; Eds., Vol. 4006, 321–327

Baldwin, J., Beckett, M., Boysen, R., Burns, D., Buscher, D., Cox, G., Haniff, C., Mackay, C., Nightingale, N., Rogers, J., Scheuer, P., Scott, T., Tuthill, P., Warner, P., Wilson, D., & Wilson, R. 1996, A&Ap, 306, L13

Baldwin, J. E., Haniff, C. A., Mackay, C. D., & Warner, P. J. 1986, Nature, 320, 595

Benson, J., Hutter, D., Elias, N. M., I., Bowers, P. F., Johnston, K. J., Hajian, A. R., Armstrong, J. T., Mozurkewich, D., Pauls, T. A., Rickard, L. J., Hummel, C. A., White, N. M., Black, D., & Denison, C. 1997, AJ, 114, 1221

Beuzit, J.-L., Mouillet, D., Oppenheimer, B. R., & Monnier, J. D. 2006, in Protostars and Planets V

Cornwell, T. J. 1987, A&Ap, 180, 269

Danchi, W. C., Tuthill, P. G., & Monnier, J. D. 2001, ApJ, 562, 440

Esposito, S., Riccardi, A., & Femenía, B. 2000, A&Ap, 353, L29

Haniff, C. A., Mackay, C. D., Titterington, D. J., Sivia, D., & Baldwin, J. E. 1987, Nature, 328, 694

Jennison, R. C. 1958, MNRAS, 118, 276+

Lachaume, R. 2003, A&Ap, 400, 795

Lane, B. F. & Colavita, M. M. 2003, AJ, 125, 1623

Lane, B. F., Colavita, M. M., Boden, A. F., & Lawson, P. R. 2000, in Proc. SPIE Vol. 4006, p. 452-458, Interferometry in Optical Astronomy, Pierre J. Lena; Andreas Quirrenbach; Eds., Vol. 4006, 452–458

Millan-Gabet, R., Monnier, J. D., Berger, J.-P., Traub, W. A., Schloerb, F. P., Pedretti, E., Benisty, M., Carleton, N. P., Haguenauer, P., Kern, P., Labeye, P., Lacasse, M. G., Malbet, F., Perraut, K., Pearlman, M., & Thureau, N. 2006, ApJL, 645, L77

Monnier, J. 2002, in Eurowinter School: Observing with the Very Large Telescope Interferometer

Monnier, J. D. 2000, in Principles of Long Baseline Stellar Interferometry, 203–+

Monnier, J. D. 2003, Reports of Progress in Physics, 66, 789

Monnier, J. D., Berger, J.-P., Millan-Gabet, R., Traub, W. A., Schloerb, F. P., Pedretti, E., Benisty, M., Carleton, N. P., Haguenauer, P., Kern, P., Labeye, P., Lacasse, M. G., Malbet, F., Perraut, K., Pearlman, M., & Zhao, M. 2006a, ApJ, 647, 444

Monnier, J. D., Danchi, W. C., Hale, D. S., Tuthill, P. G., & Townes, C. H. 2000, ApJ, 543, 868

Monnier, J. D., Pedretti, E., Thureau, N., Berger, J.-P., Millan-Gabet, R., ten Brummelaar, T., McAlister, H., Sturmann, J., Sturmann, L., Muirhead, P., Tannirkulam, A., Webster, S., & Zhao, M. 2006b, in Advances in Stellar Interferometry. Edited by Monnier, John D.; Schöller, Markus; Danchi, William C.. Proceedings of the SPIE, Volume 6268, pp. (2006).

Monnier, J. D., Traub, W. A., Schloerb, F. P., Millan-Gabet, R., Berger, J.-P., Pedretti, E., Carleton, N. P., Kraus, S., Lacasse, M. G., Brewer, M., Ragland, S., Ahearn, A., Coldwell, C., Haguenauer, P., Kern, P., Labeye, P., Lagny, L., Malbet, F., Malin, D., Maymounkov, P., Morel, S., Papaliolios, C., Perraut, K., Pearlman, M., Porro, I. L., Schanen, I., Souccar, K., Torres, G., & Wallace, G. 2004, ApJL, 602, L57

Mourard, D., Bosc, I., Labeyrie, A., Koechlin, L., & Saha, S. 1989, Nature, 342, 520

Muterspaugh, M. W., Lane, B. F., Konacki, M., Burke, B. F., Colavita, M. M., Kulkarni, S. R., & Shao, M. 2005, AJ, 130, 2866

Pauls, T. A., Young, J. S., Cotton, W. D., & Monnier, J. D. 2005, PASP, 117, 1255

Quirrenbach, A. 2000, in Principles of Long Baseline Stellar Interferometry, 71–+

Readhead, A., Nakajima, T., Pearson, T., Neugebauer, G., Oke, J., & Sargent, W. 1988, AJ, 95, 1278

Roddier, F. 1986, Optics Communications, 60, 145+

Rogstad, D. H. 1968, Applied Optics, 7, 585+

Segransan, D. 2002, in SF2A-2002: Semaine de l'Astrophysique Francaise

Shao, M. & Colavita, M. M. 1992a, ARAA, 30, 457

—. 1992b, A&Ap, 262, 353

Stee, P., de Araujo, F. X., Vakili, F., Mourard, D., Arnold, L., Bonneau, D., Morand, F., & Tallon-Bosc, I. 1995, A&Ap, 300, 219

Thompson, A. R., Moran, J. M., & Swenson, G. W. 2001, Interferometry and synthesis in radio astronomy (Interferometry and synthesis in radio astronomy by A. Richard Thompson, James M. Moran, and George W. Swenson, Jr. 2nd ed. New York : Wiley, c2001.xxiii, 692 p. : ill. ; 25 cm. "A Wiley-Interscience publication." Includes bibliographical references and indexes. ISBN : 0471254924)

Tuthill, P. & Monnier, J. 2000, Imaging and Fourier Coverage: Mapping with Depleted Arrays, Tech. Rep. 86, CHARA Array, Georgia State University,

Atlanta, GA
Tuthill, P. G., Monnier, J. D., & Danchi, W. C. 2001, Nature, 409, 1012
Tuthill, P. G., Monnier, J. D., Danchi, W. C., Wishnow, E. H., & Haniff, C. A. 2000, PASP, 112, 555
Weigelt, G., Petrov, R. G., Chesneau, O., Davidson, K., Domiciano de Souza, A., Driebe, T., Foy, R., Fraix-Burnet, D., Gull, T., Hillier, J. D., Hofmann, K.-H., Kraus, S., Malbet, F., Marconi, A., Mathias, P., Monin, J.-L., Millour, F., Ohnaka, K., Rantakyrö, F., Richichi, A., Schertl, D., Schöller, M., Stee, P., Testi, L., & Wittkowski, M. 2006, in Advances in Stellar Interferometry. Edited by Monnier, John D.; Schöller, Markus; Danchi, William C.. Proceedings of the SPIE, Volume 6268, pp. (2006).
Weigelt, G. P. 1977, Optics Communications, 21, 55
Weiner, J., Tatebe, K., Hale, D. D. S., Townes, C. H., Monnier, J. D., Ireland, M., Tuthill, P. G., Cohen, R., Barry, R. K., Rajagopal, J., & Danchi, W. C. 2006, ApJ, 636, 1067
Zhao, M., Monnier, J. D., Torres, G., & others. 2007, ApJ, in press